High Energy Processes in Accreting Black Holes
ASP Conference Series, Vol. 161, 1999
Juri Poutanen and Roland Svensson, eds.

Compton Reflection and Iron Fluorescence in Active Galactic Nuclei and Galactic Black Hole Candidates

C. S. Reynolds[1]

JILA, University of Colorado, Boulder CO80309–0440, USA.

Abstract. Any cold, optically-thick matter in the vicinity of an accreting black hole, such as the accretion disk, can intercept and reprocess some fraction of the hard X-ray continuum emission, thereby imprinting atomic features into the observed spectrum. This process of 'X-ray reflection' primarily gives rise to a broad reflection 'hump' peaking at $\sim 30\,\mathrm{keV}$ and an iron emission line at $6.4\,\mathrm{keV}$. In this review, I briefly describe the physics of this process before reviewing the observations of these features in active galactic nuclei (AGN) and Galactic black hole candidates (GBHCs). In some AGN, Seyfert galaxies in particular, the iron line is found to be very broad and asymmetric. It is believed that such lines arise from the innermost regions of the accretion disk, with mildly-relativistic Doppler shifts and gravitational redshifts combining to produce the line profile. Hence, such lines give us a direct observational probe of the region within several gravitational radii of the black hole. The complications that plague similar studies of GBHCs, such as disk ionization and the possibly of inner disk disruption, are also addressed. I conclude with a discussion of iron line reverberation, i.e. temporal changes of the iron line as 'echos' of large X-ray flares sweep across the accretion disk. It is shown that interesting reverberation effects, such as a definitive signature of extremal Kerr geometry, is within reach of high throughput spectrometers such as *Constellation-X*.

1. X-ray Reflection Features

The environment of an accreting black hole can contain optically-thick, cold matter in addition to the more exotic high-energy plasma that gives rise to the hard X-ray continuum. For example, at least some black hole accretion disks are thought to be radiatively-efficient (in the sense that they radiate locally almost all of the energy that is deposited locally by viscous processes) and hence cold. The proximity of this cold matter to the hot X-ray emitting plasma has an important consequence — the cold matter intercepts and reprocesses some fraction of the primary (featureless) X-ray continuum and hence imprints atomic features in the observed spectrum. These, the so called 'Compton reflection and

[1]Hubble Fellow

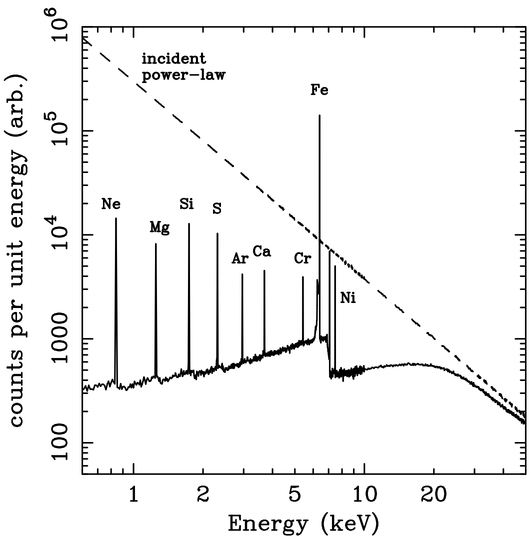

Figure 1. X-ray reflection from an illuminated slab. Dashed line shows the incident continuum and solid line shows the reflected spectrum (integrated over all angles). Monte Carlo simulation from Reynolds (1996).

iron fluorescence' features, provide a powerful probe of the accretion flow and the strong gravitational field.

In this *review*, I begin by describing the basic physical processes at work. Studies of these reprocessing features in active galactic nuclei (AGN) and Galactic Black Hole Candidates (GBHC) shall then be summarized. Finally, I discuss how future high-throughput X-ray spectrometers such as *Constellation-X* can take these studies to qualitatively new level by, for example, providing definitive signatures of rapidly and slowly rotating black holes.

2. Basic Physical Processes

The basic physics of X-ray 'reflection' can be understood by considering a hard X-ray (power-law) continuum illuminating a semi-infinite slab of cold gas. In this context, 'cold' is taken to mean that metal atoms are essentially neutral, but H and He are mostly ionized. When a hard X-ray photon enters the slab, it is subject to a number of possible interactions: Compton scattering by free or bound electrons, photoelectric absorption followed by fluorescent line emission, or photoelectric absorption followed by Auger de-excitation. A given incident photon is either destroyed by Auger de-excitation, scattered out of the slab, or reprocessed into a fluorescent line photon which escapes the slab.

Figure 1 shows the results of a Monte Carlo calculation which includes all of the above processes (Reynolds 1996; based on similar calculations by George & Fabian 1991). Due to the energy dependence of photoelectric absorption, inci-

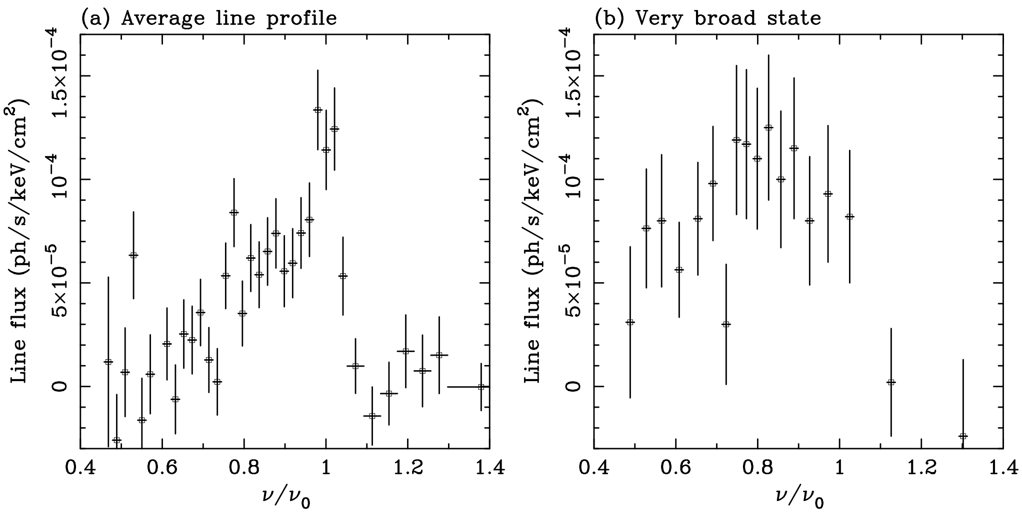

Figure 2. Iron line profiles from the long 1994 *ASCA* observation of MCG−6-30-15. Panel (a) shows the line profile from the total observation, whereas panel (b) shows the very broad state of the line found to occur during the 'deep minimum' of the lightcurve. ν_0 corresponds to the intrinsic energy of the emission line in the observers frame (6.35 keV).

dent soft X-rays are mostly absorbed, whereas hard photons are rarely absorbed and tend to Compton scatter back out of the slab. This gives the reflection spectrum a broad hump-like shape. In addition, there is an emission line spectrum resulting primarily from fluorescent Kα lines of the most abundant metals. The iron Kα line at 6.4 keV is the strongest of these lines.

For most geometries relevant to this discussion, the observer will see this reflection component superposed on the direct (power-law) primary continuum. Under such circumstances, the main observables of the reflection are a flattening of the spectrum above approximately 10 keV (as the reflection hump starts to emerge) and an iron line at 6.4 keV. For solar or cosmic abundances and a plane-parallel slab geometry, the expected equivalent width of the iron line is $150 - 200$ eV (George & Fabian 1991; Reynolds, Fabian & Inoue 1995).

3. Seyfert 1 Galaxies

Seyfert 1 nuclei appear to be the cleanest examples of the X-ray reflection at work. Low resolution spectroscopy of bright Seyfert 1 galaxies with *EXOSAT* hinted at the presence of an iron line (Nandra et al. 1989). This was confirmed by *Ginga* which also detected the spectral hardening above 10 keV indicative of the Compton reflection hump (Nandra, Pounds & Stewart 1990; Nandra & Pounds 1994). The 'reflector' was tentatively identified with the inner regions of the accretion disk, although any optically-thick and cold matter near the black hole would have created the same spectral signatures.

3.1. The ASCA Era

A breakthrough came with the launch of *ASCA* and its medium-resolution CCD spectrometers. A long (4.5 day) observation of the bright Seyfert galaxy MCG−6-30-15 in July-1994 allowed the iron line profile to be determined with some accuracy. The resulting line profile is shown in Fig. 2a (published by Tanaka et al. 1995). The line was found to be *extremely* broad (almost $10^5\,\mathrm{km\,s^{-1}}$ FWZI) and asymmetric in so that it possesses an extensive red-wing. Such a broad and asymmetric line is expected if the X-ray reflection is occurring in the inner regions of an accretion disk — strong line-of-sight Doppler shifts, transverse Doppler shifts and gravitational redshifts combine to produce an extensive low-energy wing and a sharp truncation of the line at high-energies (Fabian et al. 1989). Tanaka et al. (1995) showed that the MCG−6-30-15 data is in good agreement with the disk model provided the inclination of the disk is $\theta \approx 27^\circ$ and line fluorescence occurs down to $6r_{\mathrm{g}}$[1], the innermost stable orbit around a Schwarzschild black hole. *This result is the best evidence to date for a radiatively-efficient accretion disk around a black hole in any object.*

Subsequent studies of large samples of objects by Nandra et al. (1997a; hereafter N97) confirmed the presence of these features in many other Seyfert 1 galaxies, and show that there is a tendency for the iron lines to indicate face-on accretion disks (as expected for Seyfert 1 nuclei from the unified Seyfert scheme).

3.2. The Spin of the MCG−6-30-15 Black Hole

A more detailed examination of the MCG−6-30-15 data by Iwasawa et al. (1996a; hereafter I96) revealed a fascinating result. The red-wing of the iron line became much more extensive, and the equivalent width of the line dramatically increases when the source enters a low flux state (termed the 'deep minimum' state). This line profile is shown in Fig. 2b. Indeed, the line becomes so red that, within the context of axisymmetric emission models, one must consider line emission from within $6r_{\mathrm{g}}$. Since this is within the radius of marginal stability for a non-rotating (Schwarzschild) black hole, I96 suggest this as evidence for a rapidly rotating (near-extremal Kerr) black hole (also see Dabrowski et al. 1997). Iron line profiles from disks around near-extremal Kerr holes have been calculated by Laor (1991) and agree well with the line profile seen in the very broad state of the MCG−6-30-15 line.

However, such arguments do not account for fluorescence from plunging material within the innermost stable orbit. In fact, if the illuminating primary X-ray source is somewhat displaced from the disk plane, and the efficiency of X-ray production is low, this region can produce significant redshifted iron line emission. When emission from this region is accounted for, even a Schwarzschild black hole (or, more physically, a slowly rotating Kerr black hole) can explain the I96 result with the high-latitude X-ray source becoming more concentrated towards the centre of the disk during the deep minimum state (Reynolds & Begelman 1997; hereafter RB97). Within the RB97 model, gravitational focusing of X-rays from the primary source also accounts for the observed changes

[1] As is standard practice, we define the gravitational radius to be $r_{\mathrm{g}} = GM/c^2$, where M is the mass of the black hole.

in iron line equivalent width. Young, Ross & Fabian (1998) note that, within this scenario, a large iron edge would be produced by reflection from the ionized regions of the very innermost disk ($r < 4r_{\rm g}$). However, until the Young et al. models are formally *fitted* to the current data (with model parameters that are allowed to vary away from the best fit values of RB97), the presence or absence of this edge cannot be used to rule out the Schwarzschild model for MCG−6-30-15.

Whilst we are not in a position to claim a measurement of the spin-parameter of this black hole, it is exciting that we are debating details of the accretion flow within $r < 6r_{\rm g}$ from an observational stance.

As a word of caution in this debate, Weaver & Yaqoob (1998) have recently noted that the very broad state of the MCG−6-30-15 iron line has a poorly determined profile (due to limited photon statistics). In particular, line emission from the region $r < 6r_{\rm g}$ is not required by the data if one considers non-axisymmetric obscuration of line emitting regions of the disk. They consider a model in which an obscuring cloud eclipses the inner regions of the accretion disk. This eclipse produces both the deep minimum in the light curve (McKernan & Yaqoob 1998) as well as changing the observed line profile in the sense seen by I96. Even if such a model is considered to be ad-hoc (it requires optically-thick blobs with very well defined edges to be propelled to large distances above the disk plane), it must be addressed by further work if we wish to make a robust case that we are observing emission within $r < 6r_{\rm g}$.

3.3. Alternative Viewpoints — a Broad Line from Comptonization?

The claim that iron line studies are probing the region within a few gravitational radii of the black hole is a bold one, and should be tested against other models at every opportunity. Furthermore, the internal consistencies of the accretion disk hypothesis must be critically examined. Given the quality of data, the July-1994 MCG−6-30-15 line profile has become a testbed for such comparisons.

Fabian et al. (1995) examined many alternative models including lines from mildly relativistic outflows, the effect of absorption edges on the observed spectrum, and broadening of the line via Comptonization. Fabian et al. found that none of these models were viable alternatives for the MCG−6-30-15 line profile.

Not to be deterred, Misra & Kembhavi (1998) have recently re-examined the Comptonization model for the broad iron line and claim to succeed in reproducing the iron line profile without the need for a relativistic accretion disk. In their model, the iron line source is surrounded by a cloud with radius $R \sim 10^{14}$ cm. Compton downscattering of line photons as they pass through this cloud produces the broad, redshifted line. The cloud must be highly ionized (to avoid photoelectic absorption of all line photons) and have a temperature less than $kT \lesssim 0.2\,{\rm keV}$ (to produce mainly Compton downscattering). Hence, the radiation source ionizing this cloud has to be extremely soft with a very large optical/UV excess. However, this model possesses severe problems. Firstly, the optical/UV excess cannot possibly be as large as required in this scenario: such luminosity would either be seen directly with optical/UV observations, or would be reprocessed into the IR by dust. Either way, it could not be hidden from observers and would violate measured IR/optical/UV limits by an order of magnitude (c.f. Fig. 4 of Reynolds et al. 1997 with Fig. 1 of Misra & Kembhavi 1998). Secondly, in any reasonable geometry the primary continuum radiation would have to pass through the same Comptonizing cloud. This would produce a spectral break at $\sim 20\,\mathrm{keV}$, in contradiction to hard X-ray observations. Also, any variability of the central source would be smeared out as the photons random walk through the cloud on a timescale of

$$t_{\mathrm{var}} \sim \frac{R\tau}{c} \tag{1}$$

where τ is the optical depth of the cloud, and c is the speed of light. In the Misra & Kembhavi model, $\tau \sim 5$. Hence, one could not observe significant variability on timescales shorter than $\sim 10^4$ s. MCG−6-30-15 is frequently seen to undergo continuum changes on much more rapid timescales (down to $\sim 10^2$ s; Yaqoob et al. 1997). Hence, the observed variability timescales cannot be accommodated within this model.

4. Intermediate Seyferts and Seyfert 2 Galaxies

According to the unified scheme (e.g. Antonucci 1993), Seyfert 2 galaxies should display very similar X-ray properties to Seyfert 1 galaxies but with additional absorption from the putative molecular torus. Hence, we expect Seyfert 2 galaxies to possess accretion disk reflection spectra as do Seyfert 1 galaxies. However, because the central engines of Seyfert 2 galaxies are heavily absorbed, additional spectral components become relatively more important and can serve to make Seyfert 2 X-ray spectra complex. The exact spectrum depends sensitively on the amount of absorption.

For Seyfert 2s with relative low absorbing column densities ($N_{\mathrm{H}} \lesssim 10^{22}\,\mathrm{cm}^{-2}$), central engine emission can penetrate the absorption at energies above a few keV. In these cases, broad iron lines are often seen (Iwasawa et al. 1996b; Weaver et al. 1997; Turner et al. 1998). As in Seyfert 1 nuclei, these broad lines are thought to originate from the inner regions of the accretion disk. Whilst the reflection hump can be observationally challenging to detect against the absorbed spectrum, this also seems to be present as expected in at least some sources (e.g. see *RXTE* detection of the reflection continuum in MCG-5-23-16; Weaver et al. 1998).

A recent stir has been caused by Turner et al. (1998) who claim that the iron line profiles of these low-absorption Seyfert 2 galaxies indicate face-on accretion disks. This is in direct contradiction with unified Seyfert schemes. Furthermore, given that N97 showed Seyfert 1 galaxies to also be face-on, this results would imply an entire class of edge-on systems which are currently absent from known samples. However, Weaver & Reynolds (1998) showed that the inclusion of a narrow iron line component invalidates the Turner et al. conclusion. Such a narrow line component is expected to arise from fluorescence by the molecular torus (Krolik, Madau & Zycki 1994). Thus, iron line studies of Seyfert 2 galaxies are consistent with the unified scheme.

In high absorption Seyfert 2 systems ($N_{\mathrm{H}} \gtrsim 10^{25}\,\mathrm{cm}^{-2}$), the central engine emissions are completely blocked by the Compton thick absorber. In these cases, *ASCA* often observes a very flat continuum with a large equivalent width

($\sim 1\,\mathrm{keV}$) narrow iron line. This is interpreted as being an almost pure reflection spectrum (Fukazawa et al. 1994; Reynolds et al. 1994; Matt et al. 1996), possibly from the illuminated inner edges of the torus. The fluorescence lines from low-Z elements can also been seen in these reflection dominated cases.

5. Other Classes of AGN

For completeness, I shall briefly describe reflection studies of other classes of AGN. Firstly, luminous quasars shall be addressed. Nandra et al. (1995) found no reflection features in the two $z \sim 1$ quasars PG 1634+706 and PG 1718+481. Since any reflection features are redshifted into more sensitive parts of the *ASCA* band, good upper limits were set on the iron line and reflection continuum which effectively ruled out a Seyfert like reflection spectrum. In a complementary study, Nandra et al. (1997b) examined a sample of AGN with a variety of luminosities and found that iron lines become systematically weaker as more luminous objects were considered. One plausible explanation for this trend is that higher luminosity sources may be accreting at a larger fraction of the Eddington limit causing their inner accretion disks to be more ionized (Matt, Fabian & Ross 1993, 1996). The ionization would, in turn, lead to weaker reflection signatures. One concern regarding this explanation is that it requires a fairly small range of AGN black hole masses so that the Eddington ratio primarily determines the luminosity.

Secondly, radio-loud AGN also appear to possess reflection features which differ from the Seyfert galaxy case. Both the reflection continua and iron lines in FR-II radio galaxies are weak. The strength of the reflection continuum can be measured in terms of the $\mathcal{R}$ parameter, defined as

$$\mathcal{R} = \frac{\Omega}{2\pi} \tag{2}$$

where Ω is the solid angle subtended by the reflector at the X-ray source. In FR-II sources, it is typically found that $\mathcal{R} = 0.2 - 0.4$ (Zdziarski et al. 1995; Wozniak et al. 1998). Seyfert galaxies typically have $\mathcal{R} \sim 1$. The reason for this difference is unclear — possibilities include dilution of a Seyfert-like reflection continuum by a featureless beamed component from the relativistic radio jet, or a transition to a hot (advective?) accretion mode within some given radius. Very little is known about X-ray reflection features in FR-I radio galaxies. Their low-luminosities, coupled with the fact that nearby examples are embedded in clusters of galaxies, makes it very difficult to obtain a quality nuclear X-ray spectrum.

6. Galactic Black Hole Candidates

I now turn to stellar mass accreting black holes. This discussion will be brief and details will be deferred to the relevant papers presented at this meeting (in particular, those of C. Done, K. Ebisawa, E. Grove, P. Zycki). At first glance, the prospects for using reflection signatures to probe these sources might seem rather better than for the AGN case, since bright GBHCs are 10^3 times brighter than bright AGN. However, the reflection signatures from GBHC are rather complex, and their interpretation is still actively debated.

Many of the complications of GBHCs are illustrated by considering the famous source Cygnus X-1. Ebisawa (1991) found spectral features in the *Ginga* spectrum of Cygnus X-1 and interpreted them in terms of reflection features. Done et al. (1992) fitted ionized reflection models to *EXOSAT* and HEAO 1-A2 data, and showed that a disk with an ionization parameter of $\xi \sim 100\,\mathrm{erg\,s^{-1}\,cm}$ is a significantly better description of the data. Shifts in the strengths and energies of the absorption edges and emission lines are the main signatures of ionized reflection. It is not surprising that disks in GBHCs are more highly ionized than in AGN — simple Shakura & Sunyaev (1973) accretion disk models suggest that the thermal disk radiation from a stellar mass black hole is sufficiently energetic ($kT \sim 1\,\mathrm{keV}$) so as to partially photoionize the disk (Matt, Fabian & Ross 1993, 1996). Radial ionization gradients within the disks are also expected to exist and can have observable effects (Zycki, Done & Smith 1998).

As well as being ionized, the overall strength of the reflection continua and iron lines in GBHCs is small. Fitting (ionized) reflection models to Cygnus X-1 (Done et al. 1992) and other GBHCs implies a reflection strength of $\mathcal{R} \sim 0.2-0.4$ (similar to the value found in FR-II radio galaxies). This probably indicates that the inner accretion disk of GBHCs is not well described by the geometrically-thin, radiatively-efficient disk models of Shakura-Sunyaev and, instead, has a hot, geometrically-thick structure. The advection dominated accretion flow (ADAF) models of Narayan & Yi (1995) are an example of such a structure. In such models, a standard Shakura-Sunyaev disk exists outside of some transition radius and reflection features arise by oblique illumination of this outer disk by the central hot disk. Of course, this explanation for the low value of $\mathcal{R}$ found in GBHCs raises the following fundamental question — why do Seyfert nuclei appear to possess cold, thin accretion disks all of the way down to the innermost stable orbit, whereas GBHCs seem to require a disruption of this thin disk at relatively large distances from the black hole? What aspect of the accretion physics fails to scale when going from the stellar mass black hole case to the supermassive black hole case?

The final complication relevant to GBHCs is that the Doppler/gravitational smearing of the Compton reflection continuum can be seen (Zycki, Done & Smith 1997, 1998). Of course, such an effect should also be present in AGN, but only observations of GBHCs currently have enough signal-to-noise to allow the smearing of the reflection continuum to be discerned. Since realistic emissivity laws are highly weighted towards the centre of the disk, the predicted blurring of the reflection spectrum is a sensitive function of the inner edge of the reflecting parts of the accretion disk r_{in}, (i.e. the transition radius at which the hot inner disk begins). Hence, fitting such models to real data allows r_{in} to be constrained. Typical values are between $r_{\mathrm{in}} = 20 - 100r_{\mathrm{g}}$.

Combining these probes of the disk ionization, geometry, and dynamics is a powerful way of testing physical models for GBHCs. For example, modeling the reflection spectrum of a source at different times whilst it is undergoing a spectral state transition can directly test many of the models for such state transitions, such that of Esin, McClintock & Narayan (1997). See P. Zycki's contribution to this meeting for a discussion of these investigations.

7. The Future: X-ray Reverberation Mapping

The rapid X-ray variability of many Seyfert galaxies leads us to believe that the primary X-rays are emitted during dramatic flare-like events in the accretion disk corona. When a new flare becomes active, the hard X-rays from the flare will propagate down to the cold disk and excite iron fluorescence. Due to the finite speed of light, the illumination from the flare sweeps across the disk, and the reflected X-rays act as an 'echo' of this flare. Such flaring will cause temporal changes in the iron line profile and strength due to the changing illumination pattern of the disk and, more interestingly, time delays between the observed flare and the its fluorescent echo. This latter effect is known as reverberation.

The characteristic timescale on which reverberation effects occur is the light crossing time of one gravitational radius:

$$t_{\rm g} = \frac{GM}{c^3} = 500 \left(\frac{M}{10^8\,{\rm M}_\odot} \right)\ {\rm s} \tag{3}$$

Even when observing a bright Seyfert galaxy, *ASCA* can only achieve a count rate in the iron line of $10^{-2}\,{\rm photons}\,{\rm s}^{-2}$. The long integration times required to define the line strength and profile ($\sim 1\,{\rm day}$) will average over all of these reverberation effects[2]. These time averaged studied will always have limitations. First, the length scales relevant to the time-averaged lines are expressible purely in terms of the gravitational radius $r_{\rm g}$. Thus, time-averaged line profiles alone cannot determine the absolute value of $r_{\rm g}$ and hence the mass of the black hole. Secondly, as demonstrated in Section 3.2, similar time averaged line profiles can be obtained for a variety of spin parameters depending upon the astrophysical assumptions.

Future high-throughput X-ray observatories, starting with *XMM* but maturing with *Constellation-X*, will change this situation. Reverberation signatures will be open to study, allowing the mass and spin of black holes as well as the astrophysics of the accretion flow to be probed in unprecedented detail.

Models of iron line reverberation were first computed by Stella (1990), and further developed by Matt & Perola (1992) and Campana & Stella (1993, 1995). These studies focussed on Schwarzschild black holes and had the principal goal of suggesting ways in which the black hole mass could be measured. With the hindsight of *ASCA* results, we have performed more realistic calculations of the time response of the iron line to a flaring hard X-ray source (Reynolds et al. 1998; hereafter R98). These calculations are performed in a Kerr metric (although only non-rotating and maximally rotating cases are presented) and are fully relativistic, including the gravitational focusing/redshifting of the flare emission as it propagates to the disk. Details of the calculations will not be repeated here and can be found in R98. Our goal is to determine well-defined signatures of the black hole mass, spin, and the geometry of the X-ray source.

---

[2]One might think that GBHCs provide a better opportunity to study reverberation given that they are substantially brighter than AGN (typically by factors of 10^3). However, black hole masses in these systems are typically 10^6 times smaller than in AGN. Hence, the photon flux *per light crossing time of one gravitational radius* is 10^3 times smaller in GBHCs than it is in AGN. Thus, AGN are significantly better candidates for detecting reverberation.

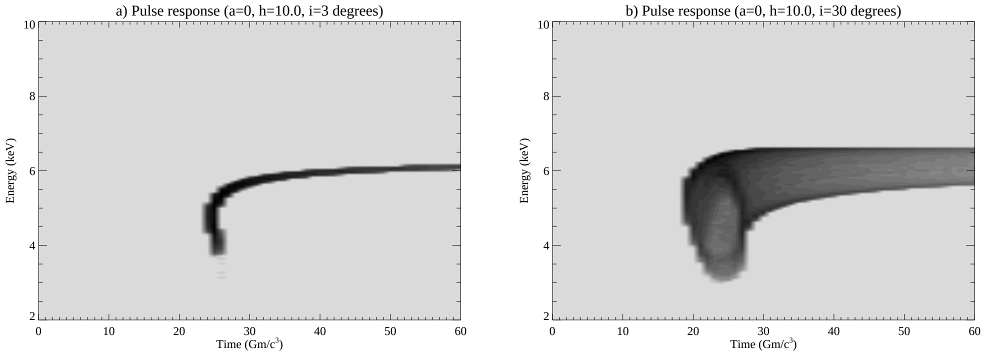

Figure 3. Transfer functions for iron line reverberation from a disk around a Schwarzschild black hole for inclinations of $i = 3^\circ$ (panel a) and $i = 30^\circ$ (panel b). The flaring source is assumed to be $10 r_{\rm g}$ above the disk plane on the symmetry axis.

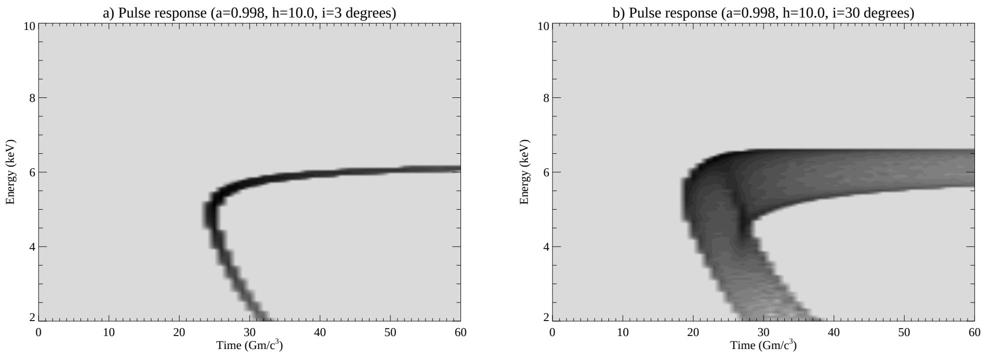

Figure 4. Same as Fig. 3, but with a maximally rotating black hole (spin parameter $a = 0.998$).

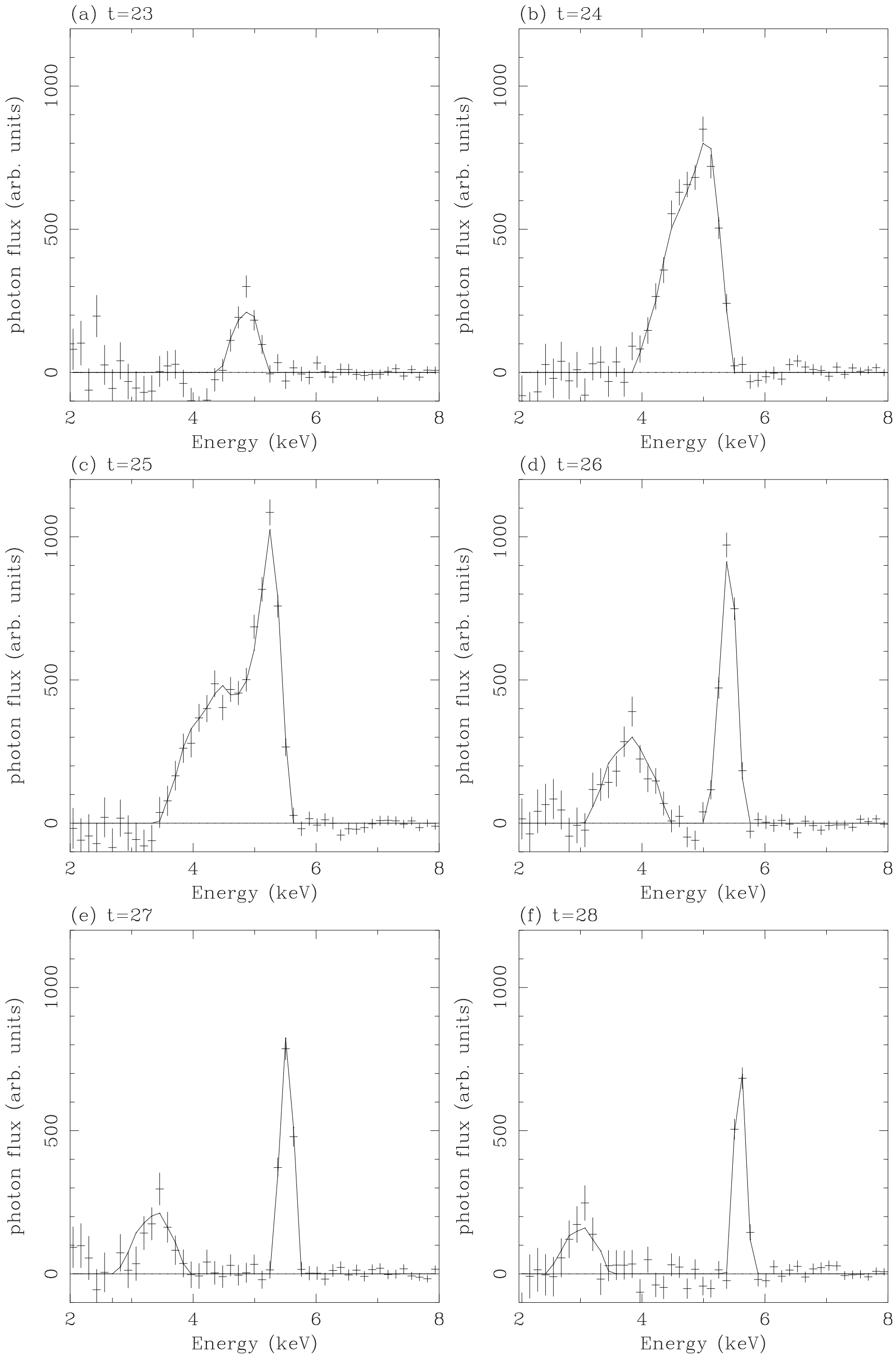

Figure 5. *Constellation-X* simulations of an on-axis reverberation events above an accretion disk around a rapidly rotating black hole. Note the bump in the spectrum. Shown here are the model (solid line) and simulated data (error bars).

The response of the line profile to an unusually large flare is considered — this approach is dictated by the fact that the general reverberation problem is not invertible due to the extended nature of the X-ray source (see R98). In the rest of this contribution, I shall summarize this study and present some new simulations which demonstrate the viability of this study with *Constellation-X*.

Figures 3 and 4 show examples of reverberation calculations for Schwarzschild and near-maximal Kerr black holes with a flare at a height of $10r_g$ above the disk plane and on the symmetry axis of the black hole/accretion disk. These figures show the transfer functions — vertical slices though the transfer function give the line profile at given times after the flare is itself is observed. Consider the almost face-on case with a Schwarzschild black hole (Fig. 3a). There is an initial delay between the observed pulse and the response in the line which is simply due to light travel times. If one were to image the disk at subsequent times, the line emitting region would be an expanding ring centered on the disk. Initially, the line emission will come from the innermost regions of the disk and will be highly redshifted by gravitational redshifts and the transverse Doppler effect. As the line-emitting region expands, these effects lessen and the observed line frequency tends to the rest-frame frequency.

As one considers higher inclination systems (e.g. Fig. 3b), line-of-sight Doppler effects come into play and the line is broadened. The time delay between the observed pulse and the line response is also shortened due to the geometry. At moderate-to-high inclinations, a generic feature appears in the line response whose presence is a direct consequence of relativity. Soon after the line profile starts responding to the observed flare, the red wing of the line fades away. During these times, the red wing of the line is due to emission from the *front* and *receding* portions of the disk, with gravitational redshifts being the dominant effect. Some time later, the observed 'echo' of the X-ray flare reaches the *back* side of the disk, whose solid angle at the observer is enhanced by lensing around the black hole itself. When the echo reaches this region, the red-wing of the line dramatically recovers before finally fading away with the rest of the line response.

A new feature appears when one considers rapidly-rotating black holes (Fig. 4). In these cases, frame-dragging by the holes rotation tends to stabilize prograde orbits around the hole. Hence, the innermost stable orbit of the accretion disk, which is assumed to be in prograde rotation with the hole, is much smaller than in the Schwarzschild case (and extends down to the horizon for extremal Kerr black holes). This immediately leads to an interesting phenomenon in the line reverberation. At a time $t > 25Gm/c^3$, the observer sees *two* rings of line emission — one is propagating outwards into the disk (as in the Schwarzschild case) and the other is propagating *inwards* towards the event horizon. This second ring corresponds to line photons that have been delayed due to their passage through the strongly curved space in the near vicinity of the hole (i.e., the Shapiro effect). This produces a small red bump in the observed line spectrum which moves progressively to lower energies as time proceeds. This effect is more prominent for flares closer to the disk. The same phenomenon accounts for the red 'tail' on the $i = 30°$ transfer function (Fig. 4b). Indeed, our calculations show these redwards moving bumps to be generic features of line reverberation around near-extremal (dimensionless spin parameter $a \gtrsim 0.9$)

Kerr holes, and hence may be considered a direct observational signatures of near-extremal Kerr geometry.

Clearly, very high-throughput spectrometers are required to perform these studies. Does *Constellation-X* have the required capabilities? To answer this question, we simulated *Constellation-X* observations of reverberation events (Young & Reynolds 1999). We considered the idealized case of an instantaneous flare occurring against a steady-state continuum. The flux and photon index of the simulated spectrum was set so as to agree with MCG$-$6-30-15. The mass of the black hole was assumed to be $10^8\,\mathrm{M}_\odot$ so that $t_\mathrm{g} = 500\,\mathrm{s}$. Also taking our lead from MCG$-$6-30-15, the normalization of the flare was such that it releases an energy equivalent to 10^4 s of the steady state continuum. The simulation was performed taking into account photon statistics in both the line and power-law continuum. The power-law continuum and a quiescent iron line (due to the stead state continuum) were subtracted from the simulated spectra in order to obtain a residual reverberating iron line profile.

Figure 5 shows a simulation for the transfer function shown in Fig. 4a (i.e. the face-on, maximal-Kerr case). Each frame shows a 1000 s integration with *Constellation-X*, and the frames are spaced $t_\mathrm{g} = 500\,\mathrm{s}$ apart. Line profile changes can be clearly tracked on these timescales. In particular, the redwards moving bump, a robust signature of a rapidly rotating black hole, can be detected and followed. We conclude that these reverberation signatures are within reach of *Constellation-X*.

8. Conclusions

In this review, I have shown how observations of X-ray Compton reflection and iron fluorescence provide a powerful probe of conditions near both stellar mass and supermassive accreting black holes. The 'cleanest' examples of X-ray reflection are found in Seyfert 1 galaxies. Medium resolution spectroscopy with *ASCA* can study the profile of the Kα iron fluorescence line. These lines are found to be very broad ($\sim 10^5\,\mathrm{km\,s^{-1}}$) and asymmetric — it is thought that a combination of Doppler shifts and gravitational redshifts produce these line profiles. Such studies indicate the presence of a thin, radiatively efficient accretion disk in the innermost regions of these AGN. Seyfert 2 galaxies also show broad iron lines. Contrary to some recent claims, iron lines in Seyfert 2s are consistent with originating in high inclination accretion disks as expected from the unified scheme. X-ray reflection is also observed in the spectra of GBHCs. However, the situation is complicated by accretion disk ionization, disrupted inner disks, and noticeable Doppler/gravitational smearing of the reflected continuum.

Future high-throughput X-ray spectrometers such as *Constellation-X* will allow reverberation effects in the iron line emission to be studied — that is, the time delay between a given X-ray flare and the corresponding X-ray reflection signatures due to the finite speed of light will be open to investigation. Strong general relativistic effects in the near vicinity of the black hole, such as extreme Shapiro delays, can cause observable iron line reverberation effects. This produces definitive signatures of extremal Kerr black holes that are within reach of future instruments such as *Constellation-X*.

Acknowledgments. The author thanks support from NASA under LTSA grant NAG5-6337, and Hubble Fellowship grant HF-01113.01-98A awarded by the Space Telescope Institute, which is operated by the Association of Universities for Research in Astronomy, Inc., for NASA under contract NAS 5-26555.

References

Antonucci R., 1993, ARAA, 31, 473

Campana S., Stella L., 1993, MNRAS, 264, 395

Campana S., Stella L., 1995, MNRAS, 272, 585

Dabrowski Y., Fabian A. C., Iwasawa K., Lasenby A. N., Reynolds C. S., 1997, MNRAS, 288, L11

Done C., Mulchaey J. S., Mushotzky R. F., Arnaud K. A., 1992, ApJ, 395, 275

Ebisawa K., 1991, PhD thesis

Esin A. A., McClintock J. E., Narayan R., 1997, ApJ, 489, 865

Fabian A. C., Rees M. J., Stellar L., White N. E., 1989, MNRAS, 238, 729

Fabian A. C. et al. 1995, MNRAS, 277, L11

Fukazawa Y. et al., 1994, PASJ, 46, L141

George I. M., Fabian A. C., 1991, MNRAS, 249, 352

Iwasawa K. et al., 1996a, MNRAS, 282, 1038 (I96)

Iwasawa K., Fabian A. C., Mushotzky R. F., Brandt W. N., Awaki H., Kunieda H., 1996b, MNRAS, 279, 837

Krolik J. H., Madau P., Zycki P. T., 1994, ApJ, 420, L57

Laor A., 1991, ApJ, 376, 90

Matt G., Perola G. C., 1992, MNRAS, 259, 433

Matt G., Fabian A. C., Ross R. R., 1993, MNRAS, 262, 179

Matt G., Fabian A. C., Ross R. R., 1993, MNRAS, 278, 1111

Matt G. et al., 1996, MNRAS, 281, L69

McKernan B., Yaqoob T., 1998, ApJ, 501, L29

Misra R., Kambhavi A. K., 1998, ApJ, 499, 205

Nandra K., Pounds K. A., 1994, MNRAS, 268, 405

Nandra K., Pounds K. A., Stewart G. C., 1990, MNRAS, 242, 660

Nandra K., Pounds K. A., Stewart G. C., Fabian A. C., Rees M. J., 1989, MNRAS, 236, 39P

Nandra K. et al., 1995, MNRAS, 276, 1

Nandra K., George I. M., Mushotzky R. F., Turner T. J., Yaqoob T., 1997a, ApJ, 477, 602 (N97)

Nandra K., George I. M., Mushotzky R. F., Turner T. J., Yaqoob T., 1997b, ApJ, 488, L91

Narayan R., Yi I., 1995, ApJ, 452, 710

Reynolds C. S., 1996, PhD thesis, University of Cambridge

Reynolds C. S., Begelman M. C., 1997, ApJ, 488, 109 (RB97)

Reynolds C. S., Fabian A. C., Inoue H., 1995, MNRAS, 276, 1311

Reynolds C. S., Fabian A. C., Makishima K., Fukazawa Y., Tamura T., 1994, MNRAS, 268, L55

Reynolds C. S., Ward M. J., Fabian A. C., Celotti A., 1997, MNRAS, 291, 403

Reynolds C. S., Young A. J., Begelman M. C., Fabian A. C., 1998, ApJ, in press (R98), astro-ph/9806327

Shakura N. I., Sunyaev R. A., 1973, A&A, 24, 337

Stella L., 1990, Nature, 344, 747

Tanaka Y. et al., 1995, Nature, 375, 659

Turner T. J., George I. M., Nandra K., Mushotzky R. F., 1998, ApJ, 493, 91

Weaver K. A., Reynolds C. S., 1998, ApJ, 503, L39

Weaver K. A., Yaqoob T., 1998, ApJ, 502, L139

Weaver K. A., Krolik J. H., Pier E. A., 1998, ApJ, 498, 213

Weaver K. A., Yaqoob T., Mushotzky R. F., Nousek J., Hayashi I., Koyama K., 1997, ApJ, 474, 675

Wozniak P. R., Zdziarski A. A., Smith D., Madejski G. M., Johnson W. N., 1998, MNRAS, 299, 449

Yaqoob T., McKernan B., Ptak A., Nandra K., Serlemitsos P. J., 1997, ApJ, 490, L25

Young A. J., Reynolds C. S., 1999, in preparation

Young A., Fabian A. C., Ross R. R., 1998, MNRAS, in press, astro-ph/9808089

Zdziarski A. A., Johnson W. N., Done C., Smith D., McNaron-Brown K., 1995, ApJ, 438, L63

Zycki P. T., Done C., Smith D., 1997, ApJ, 477, L113

Zycki P. T., Done C., Smith D., 1998, ApJ, 496, L25